Journal of Molecular Liquids 401 (2024) 124605

Contents lists available at ScienceDirect

Journal of Molecular Liquids

journal homepage: www.elsevier.com/locate/molliq

Hydration and wetting mechanism of borosilicate – Polyvinyl alcohol (PVA) hybrid aerogels of potential bioactivity

Bertold Ecsédi [a], Attila Forgács [a], Zoltán Balogh [a,b,c], István Fábián [a], József Kalmár [a,*]

[a] HUN-REN-DE Mechanisms of Complex Homogeneous and Heterogeneous Chemical Reactions Research Group, Department of Inorganic and Analytical Chemistry, University of Debrecen, Egyetem tér 1, Debrecen H-4032, Hungary
[b] Doctoral School of Chemistry, University of Debrecen, Egyetem tér 1, Debrecen, H-4032, Hungary
[c] Neutron Spectroscopy Department, HUN-REN Centre for Energy Research, Konkoly-Thege Miklós út 29-33, Budapest H-1121, Hungary

ARTICLE INFO

Keywords:
Aerogel
Hybrid material
Hydration
Wetting
NMR

ABSTRACT

Mesoporous borosilicate – polyvinyl alcohol (PVA) hybrid aerogels show positive bioactivity when interacting with dental pulp stem cells. The surface characteristics and the nanostructures of the hydrated aerogel particles are important in determining the biological response. This study reports the comparative structural characterization of pristine and stepwise hydrated hybrid aerogels, and proposes a qualitative mechanism for the wetting and pore-filling processes of these mesoporous materials. Nuclear magnetic resonance (NMR) relaxometry and cryoporometry revealed the extensive hydration of PVA macromolecules in the hybrid skeleton when contrasted to the wetting of pure silica aerogels. In spite of this extensive hydration, the open and permeable pore-structure of the hybrid borosilicate-PVA aerogels are preserved even when completely filled with liquid water. The conservation of the nanoscale architecture of the hybrid aerogels upon wetting was further confirmed by SANS. Finally, it was shown that the incorporation of microcrystalline hydroxyapatite into the hybrid skeleton does not alter the advantageous morphological features and wetting mechanism of the hybrid aerogels. The rough nanostructured skeleton is advantageous for cell binding and ensures facile mass transport through the particles in aqueous suspensions.

1. Introduction

Mesoporous aerogels prepared by drying solvated gels in supercritical CO_2 are versatile functional materials. In general, these solid materials display high porosity, low density, low thermal and electric conductivities and high compressive strength. Aerogels are intensively investigated, because they are promising for many modern industrial applications, including superior thermal insulation, catalysis, environmental management and pharmaceutics [1–5]. Naturally, the chemical composition and the nanoscale morphologies of the functional aerogels determine their macroscopic material properties, which in turn determines their performance in the targeted application.

Silica-based hybrid aerogels are of special interest in biomedical research, because of the unique combination of the properties of the inorganic and organic parts that can be utilized in drug delivery and tissue regeneration [6,7]. Solvated hybrid gels can be prepared in straightforward ways by co-gelation using the sol–gel procedure [8]. The first step in a typical sol–gel procedure is the hydrolysis and/or polycondensation of the gel precursors. This is followed by gel formation, solvent exchange and extraction with supercritical CO_2 to obtain dry aerogels. The main advantage of this procedure is that the modification of the chemical structure and the nanoscale morphology of the final aerogel can be achieved by appropriately tailoring the reaction conditions and the process parameters [9].

Borosilicate glasses and porous borosilicate matrices functionalized with different Ca(II) phosphates or apatites are promising biomaterials for bone regeneration [10,11]. In a previous study, borosilicate – polyvinyl alcohol (PVA) hybrid aerogels were synthesized and functionalized with hydroxyapatite. These mesoporous aerogels show promising biological activity when interacting with dental pulp stem cells [12]. When aerogel microparticles were added to the scratched monolayer of cells, the cells migrated towards the particles attached to them and homogeneously integrated them into the cell monolayer. It was hypothesized that the integration of the aerogel particles into the cell layer was facilitated by the nanostructured surfaces and open mesoporous structures of the aerogels, besides their advantageous chemical

* Corresponding author.
E-mail address: kalmar.jozsef@science.unideb.hu (J. Kalmár).

https://doi.org/10.1016/j.molliq.2024.124605
Received 30 January 2024; Received in revised form 22 March 2024; Accepted 28 March 2024
Available online 30 March 2024

composition. This consideration generated the need for the in-depth characterization of the surfaces and the pore structures of the hybrid aerogel microparticles in their fully hydrated states representative to the conditions in bio-fluids. For this purpose, the combination of liquid phase NMR methods and small-angle scattering techniques can be used advantageously [13–15]. Previous reports are available in the literature giving fine details on the hydration and wetting mechanisms of nano-scale porous silica materials that can serve the basis in understanding such phenomena concerning the present hybrid mesoporous aerogels [16–18].

The main goal of the present study is to investigate how the nano-structures of the different borosilicate-PVA aerogels change upon hydration and how the composition of the hybrid skeleton determine these structural changes. The effects of the incorporation of PVA macromolecules and hydroxyapatite microcrystals into the aerogel skeleton are aimed to be elucidated. Non-conventional solution phase nuclear magnetic resonance spectroscopy (NMR) methods, specifically cryoporometry and relaxometry in combination with small angle neutron scattering (SANS) measurements have been utilized for this purpose. The compiled results of these measurements provide information on the localization and distribution of water in the different chemical environments in the porous matrix, together with the concerted changes of the nanostructures of the aerogels as a consequence of wetting [19].

2. Materials and methods

2.1. Preparation of hybrid borosilicate-PVA aerogels

Three different hybrid aerogels were studied. The first aerogel is a pristine borosilicate aerogel which does not contain PVA (termed as **BS**), the second is a borosilicate-PVA hybrid aerogel (termed as **BSP**), and the third is a borosilicate-PVA aerogel functionalized with microcrystalline hydroxyapatite (termed as **BSPH**). All of these aerogels were synthesized as reported recently [12]. Briefly, the synthesis of the skeleton was achieved by co-gelation in a sol–gel procedure in all cases. Tetraethyl orthosilicate (TEOS) was dissolved in a water–ethanol mixture. This mixture was slightly acidified and stirred for 1 h before the addition of the boric acid solution. For synthesizing a hybrid skeleton, the aqueous solution of PVA was added to the TEOS and boric acid solution. In the case of the BSPH, powdered hydroxyapatite (HAp) was also added under vigorous stirring as the last component. The final step was the addition of the NH_4F catalyst to accelerate the gelation. After the addition of NH_4F, the reaction mixture was poured into a plastic mold, where the hydrolysis and polycondensation of TEOS took place in the presence of the other skeleton-forming components. After 24 h gelation, the solvent mixture was exchanged to pure ethanol, which was subsequently exchanged in multiple steps to pure acetone. Finally, acetone was extracted by supercritical CO_2 in an autoclave using a previously published two-step procedure [20]. An overview on the compositions of the aerogels is given in Table 1.

2.2. Characterization of as-prepared aerogels

The chemical characterization of the as prepared hybrid aerogels was performed using infrared spectroscopy (IR), solid state NMR (ssNMR) spectroscopy and chemical elemental analysis. The incorporation of HAp into the aerogel skeleton was confirmed by transmission electron microscopy (TEM) combined with energy-dispersive X-ray spectroscopy (EDX). The morphologies of the as-prepared aerogels were explored using low-voltage scanning electron microscopy, N_2-sorption porosimetry and small angle neutron scattering (SANS). The detailed description of the experimental procedures, instrument setups and data evaluation methods are given in details in a previous publication [12] and in the **Supporting Information (SI)**.

Table 1
The code names and the compositions of the borosilicate aerogels.

Code name	HAp content	molar ration of precursors Ca(II): TEOS: H_3BO_3	HAp: SiO_2: B_2O_3: PVA (w/w)% in aerogel
BS	–	0: 1.1: 1.0	0: 64: 36: 0
BSP	–	0: 1.1: 1.0	0: 47: 26: 27
BSPH	+	1.0: 2.3: 2.1	26: 35: 19: 20

2.3. Controlled wetting of aerogels

The as-prepared aerogel samples were gently ground and sieved to obtain ca. 200 μm particle size. These particles were hydrated using two different methods. The first method is placing the powdered aerogel into a sealed desiccator above a salt solution that controls the relative humidity of the atmosphere in the desiccator. The aerogel samples were equilibrated for 84 h under these controlled humidity conditions. The second method is directly adding liquid water to the powdered aerogel. This was realized using a micro-balance, and the designated amount of water was added in multiple aliquots under continuous but gentle mixing. These samples were sonicated in a bath type sonicator and stored for 24 h for equilibration. The final water contents of the aerogels were determined by drying at 90 °C and measuring the weight loss in a micro-balance. For SANS, pure D_2O or H_2O / D_2O mixtures were used for hydrating and wetting the aerogels.

For control, the characterization measurements were duplicated using different hydrated samples of the same nominal water contents that were either freshly prepared form dry aerogel in a single wetting step, or prepared by gradually increasing the water content of a single sample stepwise between the measurements. The point-by-point reproducibility of the NMR and SANS measurements using the independent samples was within 15 % RSD.

2.4. Characterization of hydrated aerogels

Small angle neutron scattering (SANS) measurements were performed using the same experimental setup and instrument parameters as in the case of the as-prepared aerogels. The scattering curves were evaluated using the same models, and data fitting was performed using the same methodology as for the pristine samples. All measurements were repeated at least two times using independently prepared samples.

Liquid phase NMR cryoporometry measurements were performed using the generally recommended protocols [21,22]. The sample preparation steps and the measurement parameters were optimized for the investigation of mesoporous aerogels. All measurements were repeated at least two times with independently prepared samples that were subjected to multiple melting-freezing cycles. The results were considered to be representative when the primary data were reproducible using the independent samples in repeated melting-freezing cycles. As a result, good quality data were obtained for the hybrid BSP and BSPH samples, but the hydrolytic stability of the parent BS proved to be too low for these measurements.

Liquid phase NMR relaxometry measurements were also performed. The instrument setup and measurement parameters were optimized for investigating the hydrated aerogel samples. All measurements were repeated at least twice using independently prepared sample sets, as described in Section 2.3. Robust and high quality data were obtained for hydrated BSP and BSPH, but the low hydrolytic stability of the BS sample resulted in inferior reproducibility.

The detailed description of the experimental procedures, instrument setups and data evaluation methods are given in the **SI**.

3. Results and discussion

3.1. Chemical structures of aerogels

A comprehensive IR and ssNMR study was conducted to investigate

the chemical structures of the aerogels. The detailed ssNMR results are given in Ref. [12]. The FT-IR spectra of the aerogels are shown in **Fig. S1** in the **SI**. As a summary, the characteristic peaks of the amorphous silica and boria dominate the spectrum of BS. An additional intensive peak is present around 1420 cm^{-1} in the spectra of BSP and BSPH, which is associated with the superposition of the deformation vibrations of the primary hydroxyl groups and the CH_2 groups of PVA [23]. The ssNMR results consistently show the presence of silica, boria and PVA in the hybrid skeletons. However, the existence of Si-O-B or Si-O-C bonds could not be verified unambiguously even by combining the IR and ssNMR results [24,25]. Nevertheless, the nanoscale homogeneity of the hybrid skeleton was proved using contrast-variation SANS measurements, as detailed in the next section.

Representative TEM-EDS images that display the incorporated HAp particles in the skeleton of the BSPH aerogel are shown in **Fig. S2** in the **SI**.

3.2. Morphologies of dry aerogels

High magnification SEM images of the freshly fractured surfaces of the aerogels are shown in Fig. 1. All of the studied aerogels display the classical nanoscale morphology of silica-based aerogels [16]. The skeletons are built from spherical nanoparticles less than 10 nm in size. The solid network of these interlinked nanoparticles define a highly interconnected pore system. The BS aerogel displays mainly mesopores, but few macropores are also visible in the SEM images. The hybridization of borosilicate with PVA causes the formation of large aggregates in the skeleton of BSP, which results in the formation of a significant number of macropores, as well. A similar aggregation effect has been observed earlier when silica was hybridized with biopolymers by co-gelation [18].

Interestingly, the incorporation of HAp does not cause any further visible change in the morphology. The explanation is that the shape and the size of the incorporated HAp particles are very similar to those of the aggregates in the hybrid skeleton of BSPH, as seen in the TEM-EDS images (cf. **Fig. S2** in the **SI**) [12].

Representative N_2-sorption isotherms are shown in Fig. 2. All of the hysteresis curves are IUPAC type IVa with H3 class hysteresis loops. These isotherms are characteristic for dominantly mesoporous materials with different proportions of macropores [26]. The structural parameters calculated from the isotherms based on the BET and the BJH theories are given in Table 2, and the pore size distributions are shown in Fig. 2.

The N_2-sorption results are in good agreement with the SEM observations. The morphological features of BS are practically the same as those of a typical silica aerogel. The aggregation of the primary particles in the hybrid skeleton of BSP shifts the pore size distribution toward the macropore range, but most of the pores are still smaller than 100 nm. However, the mesoporosity of BSPH is significantly reduced by the incorporation of HAp. The dominant pore sizes shift to the macropore range, and mostly outside of the quantification limit of the N_2-sorption technique. This causes the consequent decrease of the apparent surface area and the apparent pore volume in the case of BSPH.

The morphologies of the as-prepared aerogels were additionally studied by SANS [12]. The experimental scattering curves are shown in **Fig. S3** in the **SI**. These are dramatically different from each other in the low Q region, because this region is sensitive to the presence of large (50 – 100 nm wide) scattering objects. Such objects are present in the backbones of BSP and BSPH in the form of aggregates and HAp particles, but missing from the parent BS. In order to interpret these dual-scale structural features of the aerogels, the primary data were fitted by the two-level Beaucage model, as detailed in the **SI**. The fitted data at high Q values correspond to the primary particles and the mesopores of the backbone, while the fit at low Q values describes the aggregates and the macropores. The estimated structural parameters are given in **Table S1** in the **SI**. Characteristic scattering object sizes were calculated from the gyration radius (R_g) values assuming spherical geometry at both structural scales. The object sizes in the high Q region are in good agreement with the pore sizes measured by N_2-sorption, and those in the low Q region correspond roughly to the sizes of the aggregates and the HAp particles in the aerogel skeletons. The p exponent values close to 3 in the high Q region indicate that surface fractals dominate the mesoporous lower structural scale, while the values close to 4 at the higher scale show that the large objects in the skeletons have smooth surfaces [27,28].

The nanoscale architectures of the hybrid skeletons were further investigated by contrast variation SANS measurements in a previous study [12]. The aerogels were filled with H_2O:D_2O liquid mixtures, in which the H_2O:D_2O ratio was systematically varied. The contrast of the hybrid skeleton was matched with a single liquid composition (52 V/V% D_2O), which has a theoretical scattering length density (SLD) value between those of borosilicate and PVA. This is a strong indication that the hybrid backbone is homogeneous at the low nanometer scale.

3.3. Hydration and wetting of aerogels

3.3.1. Morphology of hydrated aerogels

The possibility of hydration induced morphological changes in the aerogels was studied by SANS, as detailed in a previous publication [12]. All aerogels were completely filled with D_2O, and in another set of experiments with a mixture of 8 V/V% D_2O and 92 V/V% H_2O. The latter mixture has an SLD value equivalent to that of air, therefore, it is frequently denoted as a zero-SLD probe [29,30]. Special care was taken in each case to ensure that the pore system is completely filled with the probe liquids without any air trapped inside. Thus, scattering is exclusively due to the contrast between the hydrated aerogel skeletons and the probe liquids in these experiments.

Unfortunately, it was not possible to carry out conclusive measurements with wet BS, because of the very low hydrolytic stability of this aerogel. In the case of BSP and BSPH, the experimental scattering curves of the hydrated aerogels are very similar to those of the pristine ones (Fig. 3). All curves were fitted with the two-level Beaucage model as explained in the previous section, and the estimated structural parameters are collected in Table 3.

Both the shapes of the SANS curves and the estimated structural

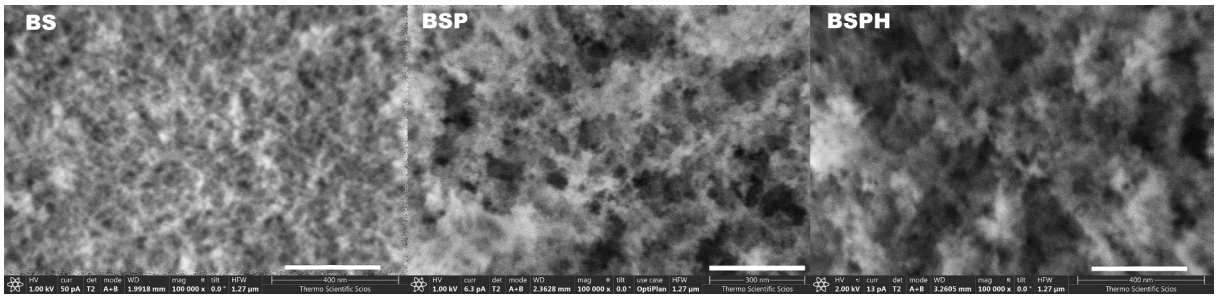

Fig. 1. Scanning electron microscopy (SEM) images of the BS, BSP and BSPH aerogels in 100 k × magnification. The scale bars are 300 nm.

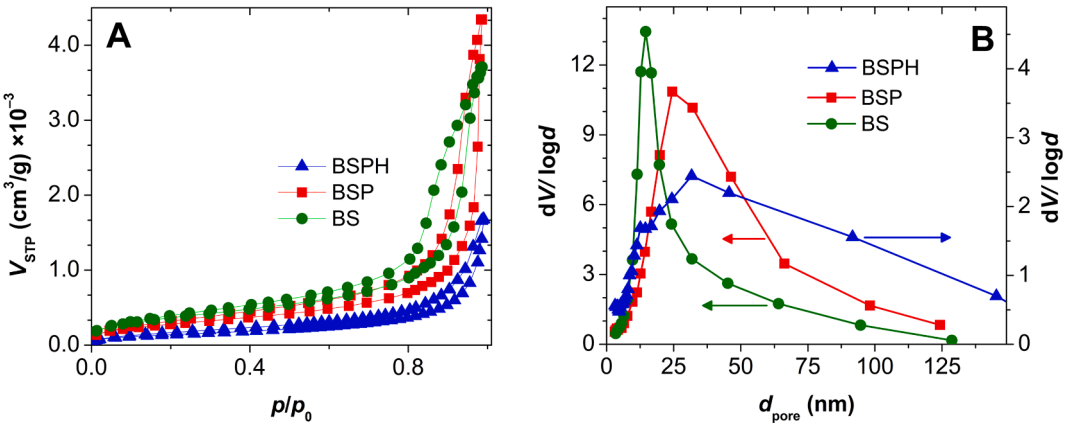

Fig. 2. Panel A: N_2 adsorption–desorption isotherms of the as-prepared aerogels. Panel B: pore size distributions calculated from the desorption isotherms using the BJH theory.

Table 2
Morphological parameters of the as-prepared aerogels calculated from the N_2-adsorption–desorption data. (The ± values are the corresponding standard deviations.).

Code name	Apparent surface area (m^2/g) / 1000	Characteristic mesopore diameter (nm)	Apparent pore volume (cm^3/g)
BS	1.3 ± 0.1	17	5.7 ± 0.2
BSP	1.0 ± 0.1	28	6.7 ± 0.3
BSPH	0.52 ± 0.05	42	2.6 ± 0.1

parameters suggest that only minor morphological changes take place upon the hydration of the hybrid aerogel skeletons. The nanoscale architecture of BSP is practically conserved at the lower structural scale, but the morphologies of the aggregates somewhat change at the higher structural scale, as indicated by the change of the corresponding *p* exponent. The value of this parameter decreases from 3.8 to 3.1 upon the hydration of the skeleton, which indicates that the interfaces of the aggregates become rough, similar to surface fractals. The characteristic features of the SANS pattern of BSPH do not change when the aerogel is hydrated. This is partly attributed to the presence of a high amount of HAp particles in the skeleton that have a major effect on the scattering. Overall, the morphologies of the HAp particles are naturally independent of hydration, resulting in a practically intact nanoscale architecture even when the hybrid aerogel is flooded with water. Nuclear magnetic resonance cryoporometry measurements were conducted on the wet aerogels with 2.5 g/g water contents to gain further morphological information on their pore systems. The relaxation filtered ^{1}H intensities of the wet aerogels are shown as a function of the temperature in Fig. 4. The marked shifts of both the melting and the freezing temperatures of water are the result of its nanoscale confinement in the solid skeletons. This is independent evidence that the pore networks of the hybrid aerogels remain open and permeable for water even under extensive hydration [18].

However, the shapes of the melting-freezing hysteresis loops in Fig. 4 are different for the two materials. The ratio of the freezing and melting temperature depressions ($\Delta T_f/\Delta T_m$) is close to 2/1 in the case of BSP, which is characteristic to continuous water bodies confined in elongated cylindrical pores. This ratio is 3/2 in the case of BSPH indicating the presence of spherical water droplets confined in the pore system [21,22]. This difference is reasonable in view of the SEM images and the N_2-sorption results, because both of these methods highlighted significant morphological differences between the aerogel skeletons. It is reasonable to assume that water can form elongated continuous bodies in the smaller interconnected pores of BSP, while the separation of larger spherical droplets is favored in the macropores of BSPH.

As described in the **SI**, the size distributions of these confined water bodies and droplets were calculated using the modified Gibbs-Thomson equation taking into account the deduced geometries (Fig. 4**B**) [21,31,32]. The cryoporometry based size distributions resulting from the melting and the freezing curves are practically the same. These sizes are in good agreement with the pore size distributions of the dry aerogels calculated from the N_2-desorption isotherms, and with the mesopore sizes estimated from the SANS data.

As a summary, the SANS and the NMR cryoporometry results are in

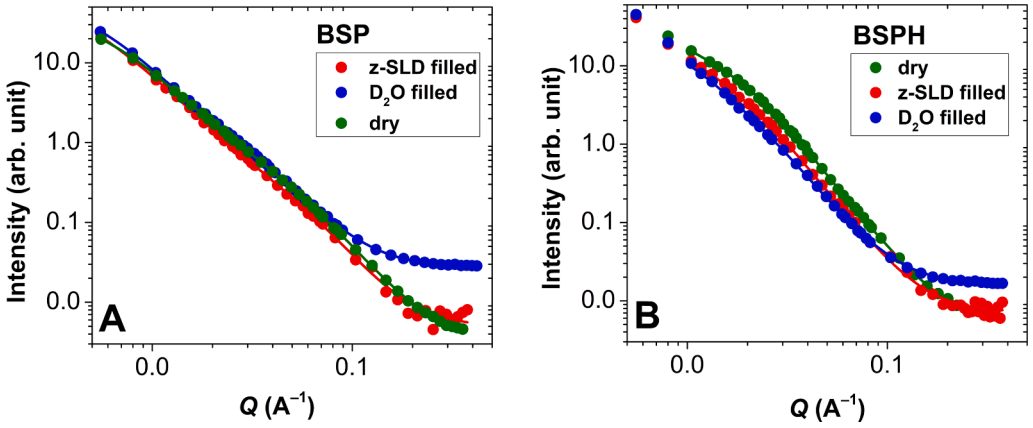

Fig. 3. Small angle neutron scattering (SANS) curves of the as-prepared and the hydrated BSP (A) and BSPH (B) samples. Markers: experimental data, lines: results of fitting.

Table 3
Structural parameters estimated from the SANS data using the two-level Beaucage model. Scattering object sizes and *p* exponents of the as-prepared and the hydrated aerogels [12]. (The ± values are the corresponding standard deviations.).

Sample	Mean object size (nm) *high Q region*	*p* exponent *high Q region*	Mean object size (nm) *low Q region*	*p* exponent *low Q region*
BSP *dry*	18 ± 1	2.9 ± 0.1	74 ± 5	3.8 ± 0.2
BSP D_2O	18 ± 1	2.9 ± 0.1	83 ± 5	3.4 ± 0.2
BSP D_2O/H_2O	18 ± 4	3.0 ± 0.2	97 ± 14	3.1 ± 0.2
BSPH *dry*	–	–	52 ± 1	3.2 ± 0.1
BSPH D_2O	–	–	49 ± 2	3.0 ± 0.1
BSPH D_2O/H_2O	–	–	52 ± 1	3.2 ± 0.1

good agreement with each other and prove in a complementary manner that the original open and interconnected mesopore networks of the aerogels are conserved in water, because the nanoscale architectures of their hybrid skeletons are practically independent of hydration.

3.3.2. *Localization of water in hydrated aerogels*

The localization of water in the different chemical environments present in the hydrated aerogels was investigated using NMR relaxometry. The spin–spin (transverse, T_2) relaxation times of water protons were measured as a function of the water contents of the materials [22].

In general, the sorption of water on amorphous silica surfaces starts with the formation of a 1–3 molecular layer thick film where the water molecules are strongly bound by H-bonds with surface silanol (Si-OH) groups. This primary water layer is termed in the literature as "strongly bound" or "non-freezing" surface water. Additional water forms a second layer atop the strongly bound molecules, which still displays restricted mobility and high molecular level order. Finally, bulk-like liquid forms on the ordered layers [33,34].

Several studies investigated the formation of thin water film inside the nanoscale pores of silicas as the first step of the pore-filling process, and described the structure of confined water. By the combination of solid state and liquid phase NMR relaxometry, cryoporometry, differential scanning calorimetry (DSC), FT-IR spectroscopy and neutron diffraction analysis, a semi-ordered water layer was identified in the pores, which is distinct from the strongly bound water [14,15,35–37]. This secondary (termed also as "freezing") water layer was detected even when the pores of amorphous silicas were completely filled with water.

When the wetting (pore-filling) process of controlled-porous silicas was investigated using liquid-phase NMR relaxometry, a distinct relaxation domain was detected with characteristically low T_2 values, different from the liquid-like pore water even close to the saturation of the pores [13,38–41]. This domain was identified as the semi-ordered water layer atop of the strongly bound water. It was shown that this semi-ordered water layer is in slow exchange with the bulk-like pore water on the timescale of the relaxometry experiments in several amorphous silicas.

In the case of the cited examples of controlled-porous silicas, the presence of physically separated pores of well-defined sizes (e.g.

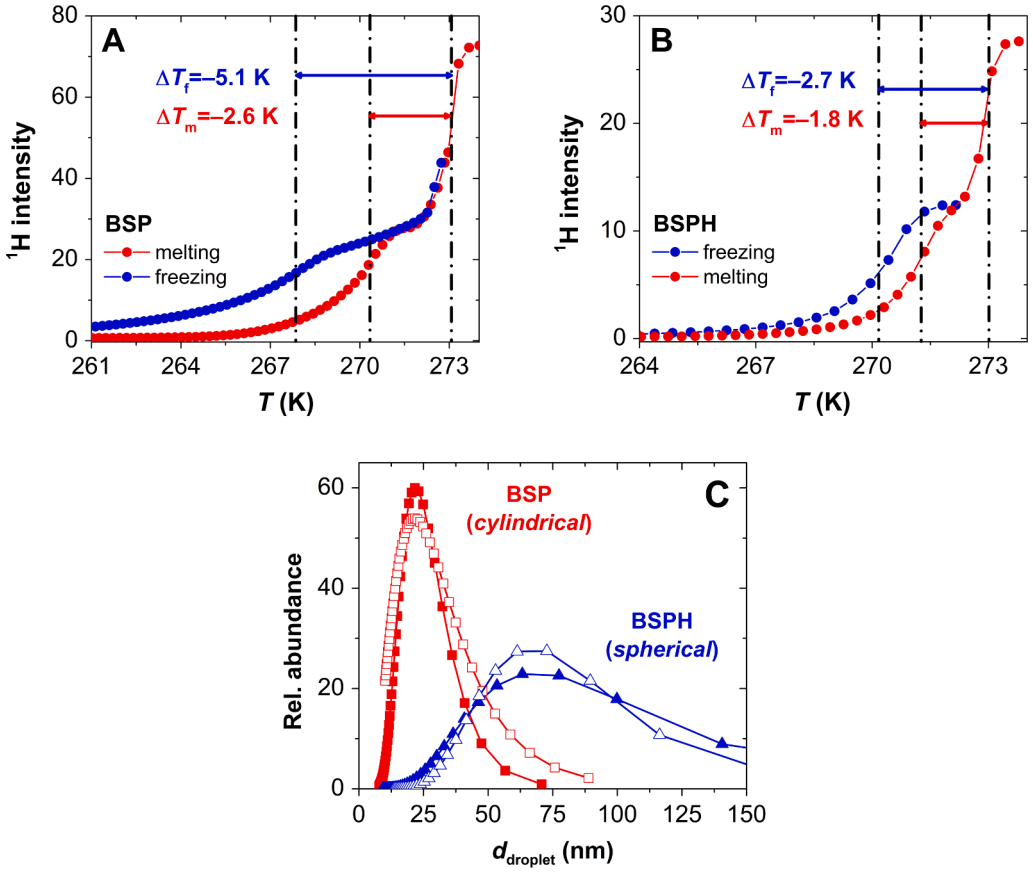

Fig. 4. Nuclear magnetic resonance (NMR) cryoporometry of hydrated BSP and BSPH at 2.5 g/g water contents. Panels A and B: Experimental melting-freezing hysteresis curves. The data points shown are the average of two series of independent experiments. Panel C: Size distributions of water bodies in the aerogels. The empty markers were calculated from the freezing curves, and the filled markers were calculated from the melting curves.

separated micropores and mesopores) are not possible, thus, the fluid in each pore cannot be considered to be magnetically isolated [42,43]. Therefore, the separate relaxation domains arise not because of the difference in the geometrical confinement in the separate pore regions, but because of the different chemical environments of the water domains in the interconnected pores. Naturally, the situation is completely different in other material families (e.g. in concretes or natural minerals) due to the distinct chemical compositions and nanoscale morphologies [44,45]. This is the reason why purely geometry based generalization is not possible for the interpretation of relaxometry data, which is emphasized in the literature [42,43].

The general tendency in the wetting and pore-filling of silica based mesoporous aerogels is as follows [46]. The strongly bound water molecules in the primary layer on the solid aerogel skeleton are not detectable by the presented liquid-phase relaxometry approach, but the protons in the semi-ordered water layer atop the primary layer are detectable and have characteristically low T_2 relaxation times [21]. After the saturation of the semi-ordered layer at higher water contents, bulk-like water builds up forming droplets in the void spaces (pores) defined by the solid skeleton. The mean T_2 relaxation times in these droplets can be magnitudes higher than in the semi-ordered surface layer depending on shape and size. Generally, the signal amplitudes of the domains are proportional to the amounts of water localized in them [17].

In the present study, two relaxation domains were identified at low water contents in BS. The characteristic T_2 values are 2 ± 1 ms and 12 ± 4 ms at 0.6 g/g water content, but the low hydrolytic stability of this material prevented its full scale investigation. Interestingly, the hydrated hybrid aerogels display three relaxation domains. The mean relaxation times measured in hydrated BSP and BSPH are shown as a function of their water contents in Fig. 5, and the corresponding amplitudes are given in **Fig. S4** in the **SI**. For comparison, the relaxation times measured under the same conditions in related silica and silica-casein aerogels are also shown in Fig. 5. [17,18].

The 1st relaxation domain with the lowest T_2 values is associated with the semi-ordered surface water layer on the aerogel skeleton. These water molecules form only a thin layer, which saturates already at low water contents. Therefore, the T_2 and the amplitude values of this domain are characteristically small, and remain constant even with the dramatic increase of the water contents of the aerogels. These features are typical of nanostructured porous silicas, including the pure silica aerogels (cf. Fig. 5**A**) [13,17,38–41].

The 3rd relaxation domain of BSP and BSPH with the highest T_2 values is associated with quasi-bulk water droplets filling the pore system. Both the T_2 values and the corresponding amplitudes of this domain increase systematically with the increase of the water contents of the aerogels. This is rational, because after the saturation of the semi-ordered water layer, all additional water is expected to accumulate in the droplets. In hydrophilic silicas, this is reflected in the steady growth of the droplet sizes until the complete filling of the pores, which causes the consequent increase of the associated T_2 values, as well as the amplitudes. Straightforward geometry based theories have been proposed to quantitatively describe the connection between the relaxation data of pore water and the physico-chemical properties of the corresponding local environments. One of the most frequently used theories in the case of silica skeletons is based on the projection of the strong surface relaxation of water into the bulk of the pores by fast exchange, which is summarized in the following equation [43,47,48].

$$\frac{1}{T_2} = \frac{1}{T_{2L}} + \lambda \frac{S_{pore}}{V_{pore}} \left(\frac{1}{T_{2S}} - \frac{1}{T_{2L}} \right) \frac{1}{f^k} \quad (1)$$

Here, T_2 is the measured relaxation time in pore water, λ is approximately the thickness of the fast relaxing primary "non-freezing" water layer on the solid surface, T_{2S} is the relaxation time in this layer and T_{2L} is the relaxation time in bulk water. Parameter f is the fraction of the pore volume that is filled with water, S_{pore} is the total apparent surface area of the porous material and V_{pore} is its total pore volume. When the solid backbone is hydrophilic and wetted evenly, the k parameter is 1, but it is lower than 1 in the case of partially hydrophobic skeletons reflecting the uneven wetting [47,49]. The corresponding $1/T_2$ vs. $1/f^k$ plot gives the expected linear trend in the case of BSP when $k = 1$, as seen in **Fig. S6** in the **SI**. However, the ca. $\lambda = 0.08$ nm value resulting from eq. (1) based on this plot is physically not realistic. The same plot gives a large negative intercept in the case of BSPH.

The above described deviation from the geometry based theory is explained by the presence of an additional relaxation domain in the hybrid aerogels compared to the pure silica aerogel. The T_2 value of this new domain (denoted as 2nd domain) is 2 ms at low water contents that increases to 7 ms at high water contents. A relaxation domain with similar T_2 values has been observed in other hybrid silica-polymer aerogels (cf. Fig. 5**A**) [17,18]. Furthermore, this domain is also missing from the parent BS aerogel. Based on these observations, the new domain in BSP and BSPH is assigned to the secondary hydration sphere of the hybrid skeleton, which consists of water molecules bound mainly to the hydrophilic PVA polymer chains. Such a secondary hydration sphere grows in size with the increase of the water content of the aerogel due to the extensive hydration and partial dissolution of the polymer chains, explaining the increase of T_2 with increasing water content. This phenomenon has been identified in the case of the hybrid silica-gelatin and silica-casein aerogels, as well [17,18].

Interestingly, while the extensive hydration causes the nanoscale

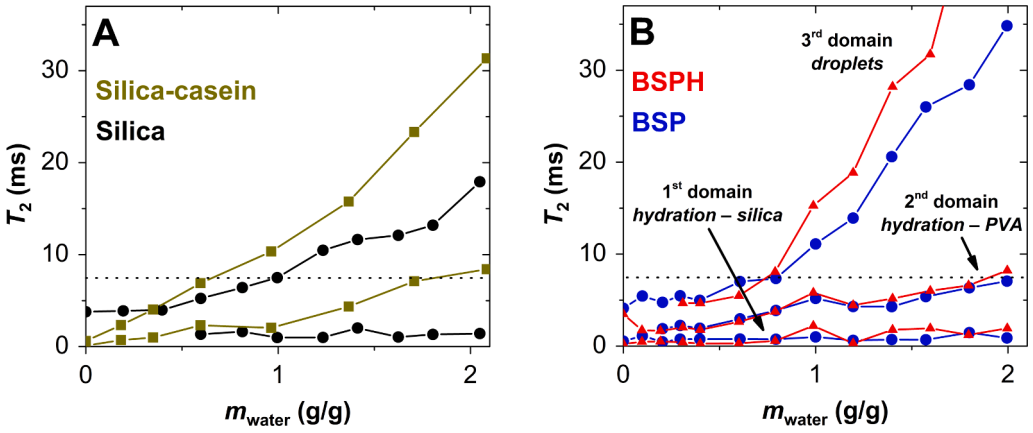

Fig. 5. NMR relaxometry of hydrated aerogels. The T_2 relaxation times measured in hydrated silica and silica-casein aerogels (A), [16,18] and those measured in hydrated BSP and BSPH (B) as a function of their water contents. The y-axis scales are the same for better comparison. The data points shown are the average of two series of independent experiments. The difference between results from the repeated experiments was less than 10%.

rearrangement of the hybrid silica-gelatin skeleton and the consequent closure of the hydrated pore system, the pore system of the hydrated silica-casein aerogels remain open and permeable in water [18]. In the case of the hybrid borosilicate-PVA aerogels, the pore system remains open, because the solid skeleton is practically intact even when completely hydrated, as shown by the combined SANS and NMR cryoporometry results. In spite of this, the wetting mechanism of the borosilicate-PVA hybrids is distinct from that of pure silica. The water molecules in the secondary hydration sphere (2^{nd} relaxation domain) and those in the droplets (3^{rd} relaxation domain) exchange with each other with rates at the low borderline of fast exchange in the timescale of the NMR relaxometry experiments, but still yield mathematically separable decays. The exchange is indicated by the correlation of the decay amplitude values estimated by the MERA data analysis. Nevertheless, the amplitudes were estimated using a pre-set number of exponential functions for fitting, and were found to be commeasurable for the last two domains. These results show that the amount of water is approximately the same in the secondary hydration sphere and in the droplets, which applies from low water contents until the filling of the pores. Interestingly, despite the extensive hydration of the hybrid backbone, the semi-ordered water layer (1^{st} relaxation domain) is still distinguishable in the borosilicate-PVA aerogels, similarly to pure silica aerogels [38].

Overall, the extensive hydration of the backbone accounts for the deviation of the operative pore-filling mechanism from the purely geometry based theory. The reason is, that such theories were laid down for nanostructured inorganic skeletons where hydration takes place only on the surface and water cannot penetrate the surface. This is not the case in the present hybrid silicas.

4. Conclusions

The wetting mechanism of amorphous silica surfaces and the pore-filling mechanisms of silica aerogels are well-known from the literature. In general, the nanoscale architecture of the silica skeleton does not change even under extensive hydration, and consequently the pore network remains open and permeable in water. However, when silica is hybridized with hydrophilic polymers, the hydration of the skeleton is significantly altered. In the case of the present borosilicate-PVA aerogels, the polymer component develops an extensive hydration sphere starting at low water contents, which exists along the semi-ordered water layer that is characteristic to amorphous silicas. The exchange of water is slow between these domains. When the water content of the hybrid aerogel is increased, water droplets start to form on the hydrated skeleton. The amounts of water in the hydration sphere of PVA and in the droplets are commeasurable, and the exchange rate is in the low borderline of fast exchange. This naturally alters the pore-filling mechanism of the hybrid aerogels compared to pure silicas. Nevertheless, the nanoscale architectures and morphologies of the hybrid skeletons are not altered by this extensive hydration, therefore, the open pore networks of the dry aerogels are conserved in water. These conclusions also apply even when nanosized hydroxyapatite particles are incorporated into the hybrid skeleton. The conservation of the pore structures of the borosilicate-PVA aerogels resemble to that of pure silica, which was unexpected, because the pores of a number of biopolymer-silica hybrids (e.g. silica-gelatin) close in water due to the extensive hydration of the backbone. An open and permeable pore network with a rough nanostructured surface is advantageous, e.g. in biomedical applications to facilitate the liquid transport through the device and the adhesion of cells on the surface.

CRediT authorship contribution statement

Bertold Ecsédi: Investigation, Formal analysis, Data curation, Conceptualization. **Attila Forgács:** Methodology, Investigation, Formal analysis, Data curation. **Zoltán Balogh:** Investigation, Formal analysis, Data curation, Conceptualization. **István Fábián:** Validation, Supervision, Resources, Funding acquisition. **József Kalmár:** Writing – original draft, Visualization, Validation, Supervision, Resources, Methodology, Investigation, Funding acquisition, Formal analysis, Conceptualization.

Declaration of competing interest

The authors declare that they have no known competing financial interests or personal relationships that could have appeared to influence the work reported in this paper.

Data availability

Data will be made available on request.

Acknowledgements

The authors are grateful for Adél Len (HUN-REN Centre for Energy Research) for the assistance in the SANS measurements, and for Zoltán Dudás (HUN-REN Centre for Energy Research) for the assistance in the synthesis procedures. This project has received funding from the HUN-REN Hungarian Research Network. The National Research, Development and Innovation Office of Hungary supported this study under grant number OTKA-139140.

Appendix A. Supplementary material

Supplementary data to this article can be found online at https://doi.org/10.1016/j.molliq.2024.124605.

References

[1] C.A. García-González, T. Budtova, L. Durães, C. Erkey, P. Del Gaudio, P. Gurikov, M. Koebel, F. Liebner, M. Neagu, I. Smirnova, Molecules 24 (2019) 1815, https://doi.org/10.3390/molecules24091815.
[2] H. Maleki, L. Duraes, C.A. Garcia-Gonzalez, P. Del Gaudio, A. Portugal, M. Mahmoudi, Adv. Colloid Interface Sci. 236 (2016) 1, https://doi.org/10.1016/j.cis.2016.05.011.
[3] I. Smirnova, P. Gurikov, J. Supercrit. Fluids 134 (2018) 228, https://doi.org/10.1016/j.supflu.2017.12.037.
[4] Z. Ulker, C. Erkey, J. Control Release 177 (2014) 51, https://doi.org/10.1016/j.jconrel.2013.12.033.
[5] G. Vasvári, J. Kalmár, P. Veres, M. Vecsernyés, I. Bácskay, P. Fehér, Z. Ujhelyi, Á. Haimhoffer, Á. Rusznyák, F. Fenyvesi, J. Váradi, Drug Discov. Today Technol. 27 (2018) 71, https://doi.org/10.1016/j.ddtec.2018.06.009.
[6] F.S. Jahed, S. Hamidi, M. Zamani-Kalajahi, M. Siahi-Shadbad, Macromol. Res. (2023) 1, https://doi.org/10.1007/s13233-023-00142-9.
[7] S. Montes, H. Maleki, Colloidal metal oxide Nanoparticles, Elsevier (2020) 337–399.
[8] L.L. Hench, J.K. West, Chem. Rev. 90 (1990) 33, https://doi.org/10.1021/cr00099a003.
[9] F. Koç, S.S. Çok, N. Gizli, F. Koc, S. Sert Cok, N. Gizli, Res. Eng. Struct. Mater. 6 (2020) 257. https://dx.doi.org/10.17515/resm2019.166ma1203.
[10] F. Baino, in: P. Palmero, F. Cambier, E. De Barra (Eds.), Advances in Ceramic Biomaterials, Woodhead Publishing, 2017, p. 249-278 10.1016/B978-0-08-100881-2.00007-5.
[11] N. Ramli, E. Sazali, Z.A. Mahraz, S. Ghoshal, S.M. Zain, R. Hisam, N. Malek, A. Syahrom, M. Sahar, F. Noor, J. Non-Cryst, Solids 609 (2023) 122289, https://doi.org/10.1016/j.jnoncrysol.2023.122289.
[12] Z. Balogh, A. Len, V. Baksa, A. Krajnc, P. Herman, G. Szemán-Nagy, Z. Czigány, I. Fábián, J. Kalmár, Z. Dudás, A.C.S. Appl, Nano Mater. 7 (2024) 4092. https://10.1021/acsanm.3c05668.
[13] A.T. Krzyżak, I. Habina, Micropor. Mesopor. Mat. 231 (2016) 230, https://doi.org/10.1016/j.micromeso.2016.05.032.
[14] J. Seyed-Yazdi, J.C. Dore, J.B.W. Webber, H. Farman, J. Phys. Condens. Matter 25 (2013) 465105, https://doi.org/10.1088/0953-8984/25/46/465105.
[15] J.B.W. Webber, Prog. Nucl. Magn. Reson. Spectrosc. 56 (2010) 78, https://doi.org/10.1016/j.pnmrs.2009.09.001.
[16] J. Kalmar, M. Keri, Z. Erdei, I. Banyai, I. Lazar, G. Lente, I. Fabian, RSC Advances 5 (2015) 107237, https://doi.org/10.1039/C5RA21353C.
[17] M. Kéri, A. Forgács, V. Papp, I. Bányai, P. Veres, A. Len, Z. Dudás, I. Fábián, J. Kalmár, Acta Biomater. 105 (2020) 131, https://doi.org/10.1016/j.actbio.2020.01.016.
[18] I. Lázár, A. Forgács, A. Horváth, G. Király, G. Nagy, A. Len, Z. Dudás, V. Papp, Z. Balogh, K. Moldován, L. Juhász, C. Cserháti, Z. Szántó, I. Fábián, J. Kalmár,

Appl. Surf. Sci. 531 (2020) 147232, https://doi.org/10.1016/j.apsusc.2020.147232.
[19] B. Zhou, Energy & Fuels 32 (2018) 8897, https://doi.org/10.1021/acs.energyfuels.8b01603.
[20] I. Lazar, I. Fabian, Gels 2 (2016) 26, https://doi.org/10.3390/gels2040026.
[21] A. Forgacs, V. Papp, G. Paul, L. Marchese, A. Len, Z. Dudas, I. Fabian, P. Gurikov, J. Kalmar, A.C.S. Appl, Mater. Interfaces 13 (2021) 2997, https://doi.org/10.1021/acsami.0c17012.
[22] M. Kéri, D. Nyul, K. László, L. Novák, I. Bányai, Carbon 189 (2022) 57, https://doi.org/10.1016/j.carbon.2021.12.045.
[23] H. Tadokoro, Bull. Chem. Soc. Jpn. 32 (1959) 1252, https://doi.org/10.1246/bcsj.32.1252.
[24] A. Irwin, J. Holmgren, J. Jonas, J. Non-Cryst, Solids 101 (1988) 249, https://doi.org/10.1016/0022-3093(88)90160-3.
[25] A.D. Irwin, J.S. Holmgren, T.W. Zerda, J. Jonas, J. Non-Cryst, Solids 89 (1987) 191, https://doi.org/10.1016/S0022-3093(87)80332-0.
[26] M. Thommes, K. Kaneko, A.V. Neimark, J.P. Olivier, F. Rodriguez-Reinoso, J. Rouquerol, K.S.W. Sing, Pure Appl. Chem. 87 (2015) 1051, https://doi.org/10.1515/pac-2014-1117.
[27] P. Debye, A.M. Bueche, J. Appl. Phys. 20 (1949) 518, https://doi.org/10.1063/1.1698419.
[28] G. Porod, Kolloid-z. 124 (1951) 83, https://doi.org/10.1007/BF01526289.
[29] L. Ludescher, R. Morak, C. Balzer, A.M. Waag, S. Braxmeier, F. Putz, S. Busch, G. Y. Gor, A.V. Neimark, N. Hüsing, G. Reichenauer, O. Paris, Langmuir 35 (2019) 11590, https://doi.org/10.1021/acs.langmuir.9b01375.
[30] R. Morak, S. Braxmeier, L. Ludescher, F. Putz, S. Busch, N. Husing, G. Reichenauer, O. Paris, J. Appl. Crystallogr. 50 (2017) 1404, https://doi.org/10.1107/S1600576717012274.
[31] V.M. Gun'ko, Appl. Surf. Sci. 307 (2014) 444 10.1016/j.apsusc.2014.04.055.
[32] J. Mitchell, J.B.W. Webber, J.H. Strange, Phys. Rep. 461 (2008) 1, https://doi.org/10.1016/j.physrep.2008.02.001.
[33] D.B. Asay, S.H. Kim, J. Phys. Chem. B 109 (2005) 16760, https://doi.org/10.1021/jp053042o.
[34] G.E. Ewing, J. Phys. Chem. B 108 (2004) 15953, https://doi.org/10.1021/jp040378+.
[35] G. Buntkowsky, H. Breitzke, A. Adamczyk, F. Roelofs, T. Emmler, E. Gedat, B. Grunberg, Y. Xu, H.H. Limbach, I. Shenderovich, A. Vyalikh, G. Findenegg, Phys. Chem. Chem. Phys. 9 (2007) 4843, https://doi.org/10.1039/B707322D.
[36] B. Grunberg, T. Emmler, E. Gedat, I. Shenderovich, G.H. Findenegg, H.H. Limbach, G. Buntkowsky, Chem. Eur. J. 10 (2004) 5689, https://doi.org/10.1002/chem.200400351.
[37] A. Vyalikh, T. Emmler, B. Grünberg, Y. Xu, I. Shenderovich, G.H. Findenegg, H. H. Limbach, G. Buntkowsky, Z. Phys, Chem. 221 (2007) 155, https://doi.org/10.1524/zpch.2007.221.1.155.
[38] S.G. Allen, P.C.L. Stephenson, J.H. Strange, J. Chem. Phys. 106 (1997) 7802, https://doi.org/10.1063/1.473780.
[39] A.T. Krzyzak, W. Mazur, J. Matyszkiewicz, A. Kochman, J. Phys. Chem. C 124 (2020) 5225, https://doi.org/10.1021/acs.jpcc.9b11790.
[40] W.E. Troyer, R. Holly, H. Peemoeller, M.M. Pintar, Solid State Nucl. Magn. Reson. 28 (2005) 238, https://doi.org/10.1016/j.ssnmr.2005.10.003.
[41] J.R. Zimmerman, B.G. Holmes, J.A. Lasater, J. Phys. Chem. 60 (1956) 1157, https://doi.org/10.1021/j150543a002.
[42] S. Davies, K.J. Packer, D.R. Roberts, F.O. Zelaya, Magn. Reson. Imaging 9 (1991) 681, https://doi.org/10.1016/0730-725X(91)90357-R.
[43] C. Schlumberger, L. Sandner, A. Michalowski, M. Thommes, Langmuir 39 (2023) 4611, https://doi.org/10.1021/acs.langmuir.2c03337.
[44] M.A. Javed, S. Komulainen, H. Daigle, B. Zhang, J. Vaara, B. Zhou, V.-V. Telkki, Micropor. Mesopor. Mat. 281 (2019) 66, https://doi.org/10.1016/j.micromeso.2019.02.034.
[45] J. Li, S. Mailhiot, A.M. Kantola, H. Niu, H. Sreenivasan, V.-V. Telkki, P. Kinnunen, Cem. Concr. Res. 160 (2022) 106921, https://doi.org/10.1016/j.cemconres.2022.106921.
[46] P. Veres, M. Kéri, I. Bányai, I. Lázár, I. Fábián, C. Domingo, J. Kalmár, Colloids Surf. B 152 (2017) 229, https://doi.org/10.1016/j.colsurfb.2017.01.019.
[47] F. Gallego-Gómez, C. Cadar, C. López, I. Ardelean, J. Colloid Interface Sci. 561 (2020) 741, https://doi.org/10.1016/j.jcis.2019.11.050.
[48] M. Simina, R. Nechifor, I. Ardelean, Magn. Reson. Chem. 49 (2011) 314, https://doi.org/10.1002/mrc.2749.
[49] U. Baig, M. Faizan, M.A. Dastageer, Adv. Colloid Interface Sci. 297 (2021) 102525, https://doi.org/10.1016/j.cis.2021.102525.